*Journal of Sound and Vibration* (1997) **201**(5), 595–611

# ACTIVE INTENSITY CONTROL FOR THE REDUCTION OF RADIATED DUCT NOISE

S.-W. KANG AND Y.-H. KIM

*Center for Noise and Vibration Control, Department of Mechanical Engineering, Korea Advanced Institute of Science and Technology, Science Town, Taejon* 305-701, *Korea*

(*Received* 13 *September* 1994, *and in final form* 14 *October* 1996)

Mean intensity based active control for the cancellation of radiated noise out of the duct exit is studied. The active intensity control strategy is derived based on the relation of the exterior sound field radiated out of the duct termination and the interior sound field of the duct. One of the characteristics of this control strategy is that the maximum possible control performance can be maintained regardless of the sensor location, compared with the conventional local pressure control methods at either interior downstream or exterior field positions. This is a simple consequence of the active intensity at the interior downstream being not space-dependent as long as it is plane wave. A time-domain adaptive filtering method for the active intensity control is also suggested and experimental results for an open ended duct based on the adaptive filtering method are presented. For the purpose of practical comparison, experimental results for conventional sound pressure control based on the well known filtered-$x$ LMS algorithm are also presented. The experimental results show the potential of the active intensity control strategy for reducing the emitted noise out of the duct exit.



## 1. INTRODUCTION

Active noise control for the reduction of duct noise has been widely investigated theoretically and experimentally with regard to various control strategies: local sound pressure control, total acoustic potential energy control, downstream potential energy control, positive-travelling pressure control, total acoustic radiation power control and acoustic power absorbing control by secondary source [1–9]. Most practical approaches of these active control strategies has been, over the last decade, based on the modified least mean square adaptive filtering technique: filtered-$x$ LMS (least-mean-square) algorithm [10]. These studies mainly treat the interior noise control problems of a duct. However, there are relatively few studies concerned with the relation between the interior noise control and the exterior noise out of the duct exit; the latter would be the major concern in many practical problems such as exhaust noise of a vehicle, or ducted fan noise.

The exterior noise from a duct exit is basically related to the termination condition and the acoustic power at its exit. The termination condition is inherently dependent on the geometrical configuration of the duct exit and the acoustic loading condition of the exterior field, so that it determines an acoustic radiation efficiency. This means that one cannot change the termination condition by a driving control source; in other words, the active control system cannot modify the radiation condition of the duct exit. However, it is noteworthy that the acoustic power at the duct exit can be controlled by a suitable downstream secondary source.

0022–460X/97/150595 + 17 $25.00/0/sv960781 

The main objective of this paper is to find the most appropriate acoustic measure to be controlled for having minimum noise from a duct exit. In this paper, the relations among the external sound pressure of duct, the radiation power out of the duct termination, sound pressures, and the active and reactive intensities at each downstream position in the duct are derived to obtain the most adequate cost function actively to be controlled. It is concluded that the active sound intensity downstream is the most proper one. A time-domain adaptive filtering method for the active intensity conrol is also suggested and experimental results for an open ended duct based on the adaptive filtering method are presented. For the purpose of practical comparison, experimental results for conventional sound pressure control based on the well known filtered-$x$ LMS algorithm [10] are also presented.

## 2. INTERNAL AND EXTERNAL SOUND FIELD OF DUCT

A typical arrangement of the ducted noise problem is illustrated in Figure 1. Without loss of generality, one can assume that there is one monopole primary source located at $x_p$ with volume velocity $q_p$ and a secondary source at $x_s$ with $q_s$. The impedances at both ends are denoted by $Z_o$ and $Z_t$ (or reflection coefficients, $R_o$ and $R_t$). The termination impedance $Z_t$ can be considered as the loading condition upon the outer acoustic field. Only a plane sound wave in the duct is considered, it being assumed that the wavelengths of interest are much longer than the characteristic length of the duct cross-section.

The internal sound pressures $p_u$ and $p_d$ upstream and downstream of the control source (see Figure 1), can be readily obtained in terms of propagating components $p_u^+$, $p_d^+$ and reflected components $p_u^-$, $p_d^-$. One has

$$p_u(x) = p_u^+(q_p, q_s)\,\mathrm{e}^{-\mathrm{j}kx} + p_u^-(q_p, q_s)\,\mathrm{e}^{+\mathrm{j}kx}, \tag{1a}$$

$$p_d(x) = p_d^+(q_p, q_s)\,\mathrm{e}^{-\mathrm{j}kx} + p_d^-(q_p, q_s)\,\mathrm{e}^{+\mathrm{j}kx}, \tag{1b}$$

where

$$p_u^+(q_p, q_s) = \frac{\rho c}{2S}\left\{\frac{R_o\,\mathrm{e}^{\mathrm{j}k(L-x_p)} + \mathrm{e}^{\mathrm{j}k(L+x_p)}}{\mathrm{e}^{\mathrm{j}kL} - R_oR_t\,\mathrm{e}^{-\mathrm{j}kL}}\,q_p + \frac{R_o\,\mathrm{e}^{\mathrm{j}k(L-x_s)} + R_oR_t\,\mathrm{e}^{-\mathrm{j}k(L-x_s)}}{\mathrm{e}^{\mathrm{j}kL} - R_oR_t\,\mathrm{e}^{-\mathrm{j}kL}}\,q_s\right\}, \tag{2a}$$

$$p_u^-(q_p, q_s) = \frac{\rho c}{2S}\left\{\frac{R_t\,\mathrm{e}^{-\mathrm{j}k(L-x_p)} + R_oR_t\,\mathrm{e}^{-\mathrm{j}k(L+x_p)}}{\mathrm{e}^{\mathrm{j}kL} - R_oR_t\,\mathrm{e}^{-\mathrm{j}kL}}\,q_p + \frac{\mathrm{e}^{\mathrm{j}k(L-x_s)} + R_t\,\mathrm{e}^{-\mathrm{j}k(L-x_s)}}{\mathrm{e}^{\mathrm{j}kL} - R_oR_t\,\mathrm{e}^{-\mathrm{j}kL}}\,q_s\right\}, \tag{2b}$$

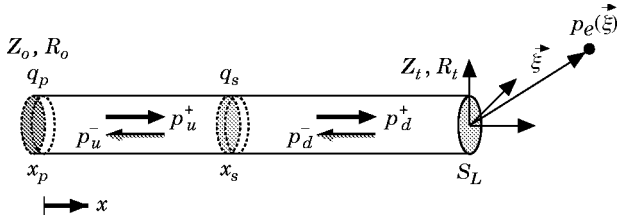


Figure 1. The internal and external sound field of a duct in which a primary source located at $x_p$ with strength $q_p$ and a secondary source at $x_s$ with $q_s$. $Z_o$, $R_o$ and $Z_t$, $R_t$ are acoustic impedances at the ends and $S_L$ is the cross-sectional area at $x = L$. $p_u^+$, $p_u^-$ and $p_d^+$, $p_d^-$ are the propagating and reflected sound pressures upstream and downstream, and $p_e(\xi)$ is the sound pressure in the exterior field.

$$p_d^+(q_p, q_s) = \frac{\rho c}{2S}\left\{\frac{R_o\, e^{jk(L-x_p)} + e^{jk(L+x_p)}}{e^{jkL} - R_o R_t\, e^{-jkL}}\, q_p + \frac{R_o\, e^{jk(L-x_s)} + e^{jk(L-x_s)}}{e^{jkL} - R_o R_t\, e^{-jkL}}\, q_s\right\}, \tag{2c}$$

$$p_d^-(q_p, q_s) = R_t\, e^{-2jkL} p_d^+(q_p, q_s) \tag{2d}$$

The subscripts $u$, $d$ and $S$ denote upstream, downstream and the cross-sectional area of the duct respectively.

The Helmholtz integral equation for the external sound field out of the duct termination is

$$p_e(\vec{\xi}) = jk\rho c \int_{S_L} u(\vec{\xi}_L) G_e(\vec{\xi} \mid \vec{\xi}_L)\, dS_L, \tag{3}$$

where $u(\vec{\xi}_L)$ and $S_L$ are the particle velocity and the cross-section area at the duct exit, respectively. The Green function $G_e$ satisfies the homogeneous Neumann boundary condition, that is $\partial G_e/\partial n = 0$ for all surfaces surrounding the duct structure. Since a plane wave field in the duct has been assumed, the velocity $u(\vec{\xi}_L)$ is uniform ($u_L$) over the duct exit area so equation (3) can be rewritten as

$$p_e(\vec{\xi}) = jk\rho c u_L \int_{S_L} G_e(\vec{\xi} \mid \vec{\xi}_L)\, dS_L = jkp_L \frac{1 - R_t}{1 + R_t} \int_{S_L} G_e(\vec{\xi} \mid \vec{\xi}_L)\, dS_L \tag{4}$$

where $p_L$ is the sound pressure at the duct exit. Thus one has expressions for internal and external sound fields, respectively, equations (1) and (4), in terms of the variables associated with a finite length duct.

## 3. ACTIVE CONTROL OF EXTERNAL SOUND FIELD

The acoustic potential energy at each external position ($e_{pe}(\vec{\xi})$) can be obtained from equation (4) as

$$e_{pe}(\vec{\xi}) = \frac{1}{4\rho c^2} |p_e(\vec{\xi})|^2 = k^2/4\rho c^2\, |p_L|^2 \left|\frac{1 - R_t}{1 + R_t}\right|^2 \left|\int_{S_L} G_e(\vec{\xi} \mid \vec{\xi}_L)\, dS_L\right|^2. \tag{5}$$

From equations (1b), (2c) and (2d), the sound pressure at the duct exit is obtained as

$$p_L = p_d(L) = p_d^+\, e^{-jkL} + p_d^-\, e^{+jkL} = p_d^+(1 + R_t)\, e^{-jkL}. \tag{6}$$

Substitution of equation (6) into equation (5) gives

$$e_{pe}(\vec{\xi}) = D(\vec{\xi})|p_d^+|^2, \tag{7a}$$

where

$$D(\vec{\xi}) = k^2/4\rho c^2\, |1 - R_t|^2 \left|\int_{S_L} G_e(\vec{\xi} \mid \vec{\xi}_L)\, dS_L\right|^2. \tag{7b}$$

Equation (7) essentially says that the acoustic potential energy density at exterior field is basically related to the propagating wave energy ($|p_d^+|^2$) at the interior downstream and it is shaped by the space-dependent factor ($D(\vec{\xi})$); that is, the "directivity pattern" that is related to the geometrical configuration of the duct exit and the exterior field condition. This result does not, of course, violate general common sense.

Keeping this fact in mind, one can now consider the downstream acoustic field from the secondary source. The acoustic potential energy density at each downstream position ($e_{pd}$), can be readily obtained from equations (1b), (2c) and (2d) as a form of space-dependent shape function ($F_1$) which represents the "standing wave pattern" of propagating wave energy ($|p_d^+|^2$).

$$e_{pd}(x) = (1/4\rho c^2)|p_d(x)|^2 = (1/4\rho c^2)|1 + R_t\, e^{-2jk(L-x)}|^2|p_d^+|^2 \equiv F_1(x)|p_d^+|^2. \tag{8}$$

The mean active sound intensity ($I_{ad}$) and the reactive sound intensity ($I_{rd}$) in the downstream field can be expressed as

$$I_{ad}(x) = \tfrac{1}{2}\,\mathrm{Re}\,[\,p_d(x)u_d^*(x)], \qquad I_{rd}(x) = \tfrac{1}{2}\,\mathrm{Im}\,[\,p_d(x)u_d^*(x)], \tag{9a, b}$$

where the particle velocity downstream ($u_d$) can be obtained from the pressure gradient by using the relation (or Euler equation)

$$u_d(x) = -(1/jk\rho c)\,\mathrm{d}p_d(x)/\mathrm{d}x. \tag{10}$$

Substitutions of equations (1), (2) and (10) into equation (9) and appropriate rearrangements yield

$$I_{ad}(x) = (1/2\rho c)(|p_d^+|^2 - |p_d^-|^2) = (1/2\rho c)(1 - |R_t|^2)|p_d^+|^2 \equiv C_1|p_d^+|^2, \tag{11a}$$

$$I_{rd}(x) = (1/\rho c)\,\mathrm{Im}\,[R_t\, e^{-2jk(L-x)}]|p_d^+|^2 \equiv F_2(x)|p_d^+|^2. \tag{11b}$$

One can see from equations (11a) that the active intensity in the duct downstream is the product of the space-independent modulus ($C_1$) and propagating wave energy, and the active intensity is always non-negative since the magnitude of the reflection coefficient ($|R_t|$) cannot be greater than unity. The reactive intensity ($I_{rd}$) is also expressed as proportional to propagating wave energy but it is shaped by the space-dependent function ($F_2(x)$).

The acoustic radiation power out of the termination ($W_r$) is also basically related to the propagating wave component in the downstream,

$$W_r = \int_{S_L} I_{ad}(L)\,\mathrm{d}S_L = S_L C_1 |p_d^+|^2. \tag{12}$$

It is noteworthy that all the above acoustic quantities are related to the propagating wave component downstream, which can be controlled by the secondary source. Therefore one can conclude that, downstream, acoustic potential energy density control and active or reactive intensity control and radiation power control out of the termination have the same effect on controlling the exterior sound field, even if the acoustical control measures are different.

It is also interesting to note that the active intensity is not space-dependent, as indicated by equation (11a). This characteristic has an important implication for practical applications: that is, intensity control can prevail against the poor observability problem that often happens and degrades the control performance in the conventional, local sound pressure control configuration which uses a pressure transducer. This fact will be investigated in more detail in terms of real-time experiments of active intensity control and sound pressure control in section 5.

The optimal control source ($q_{so}$) for the minimization of the active intensity in the interior downstream can be readily obtained from equations (11a) and (2c). It is noteworthy that the minimization of the active intensity with respect to the control source

strength does not necessarily require one to know the constant $C_1$ in equation (11a) since it is not dependent on the control source strength ($q_s$):

$$q_{so}(\omega) = -\frac{e^{j\omega x_p/c} + R_o(\omega)\, e^{-j\omega x_p/c}}{e^{j\omega x_s/c} + R_o(\omega)\, e^{-j\omega x_s/c}}\, q_p(\omega). \tag{13}$$

In equation (13), one can see that the optimal source strength is related to the two source positions $x_p$ and $x_s$ and to the upstream reflection coefficient $R_o$, but is not dependent on the downstream termination condition. If one takes the inverse Fourier transform of equation (13) and uses the binomial expansion theorem $(1+x)^{-1} = 1 - x + x^2 - x^3 + \cdots$, then the form of the optimal control source strength in the time domain becomes

$$q_{so}(t) = \sum_{i=1}^{\infty} a_i q_p(t - \tau_i), \qquad \tau_i > 0. \tag{14}$$

Equation (14) simply states that the optimal source strength is the sum of delayed versions of the primary source strength. That is, the optimal controller can be designed by a causal transversal filter.

## 4. ADAPTIVE FILTERING FOR ACTIVE INTENSITY CONTROL

To implement practically the active intensity control in a duct, the adaptive filtering algorithm in time domain, developed by Hald [11] can be used. The algorithm had been developed originally to implement the active power absorbing strategy by the control source for a general acoustic system. Therefore one could suspect that the algorithm could have potential difficulty for the present purpose, because the active intensity is not positive definite in general. However, the active intensity in the duct downstream from the control source is always non-negative as previously stated in section 3. Therefore, one can apply the adaptive filtering algorithm to implement the current active intensity control strategy.

Another possible method of implementing the active intensity control would be the frequency-domain filtered-$x$ algorithm in which one considers the imaginary part of the cross-spectrum of the two pressure measurements scaled by $\rho \Delta r \omega$, where $\rho$ is the medium's density, $\Delta r$ is the separation distance and $\omega$ is the angular frequency (that is, the active part of the sound intensity in the frequency domain) as a cost function. In recent investigation [12], the adaptive filtering algorithm in the frequency domain to implement the active intensity control strategy has been suggested. The ultimate aim of the algorithm was to control actively an enclosure sound field in which strong standing waves exist.

The above algorithms require a lengthy data averaging process and a finite-length DFT (or FFT) process respectively, which cause computational complexities in real-time control. Thus the authors have attempted to find another adaptive algorithm which is far simpler in computation. The formulation of the adaptive filtering law is similar to the active sound power absorbing algorithm [11] and sound energy density control algorithm [13]; however, the applicability and stability of the adaptive structure based on the instantaneous sound intensity for the mean (active) sound intensity control is investigated, since it is very simple in computation.

In Figure 2 is shown the block diagram of time-domain adaptive algorithm for active intensity control. Assuming stochastic process of zero mean, one can first define the

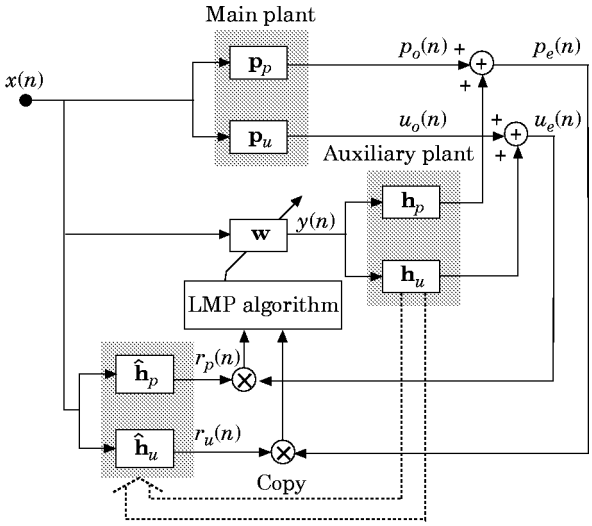


Figure 2. A block diagram of the filtered-$x$ LMP (least-mean-product) algorithm (equation (38)) for controlling active sound intensity in the duct. $\mathbf{w}$ denotes the adaptive control filter, while $\mathbf{h}_p$ and $\mathbf{h}_u$ represent auxiliary plants relating the control output $y(n)$ to the acoustic pressure $p_e(n)$ and particle velocity $u_e(n)$ at the error position. $\hat{\mathbf{h}}_p$ and $\hat{\mathbf{h}}_u$ denote the estimated copies of the auxiliary plants $\mathbf{h}_p$ and $\mathbf{h}_u$ respectively.

reference input vector $\mathbf{x}(n)$ at the discrete time step $n$, constructed with the latest $L$ successive samples of the signal $x(n)$,

$$\mathbf{x}(n) = [x(n) \quad x(n-1) \quad \cdots \quad x(n-L+1)]^{\mathrm{T}}, \tag{15}$$

and $\mathbf{w}(n)$, the adaptive transversal filter with $L$ tap weights,

$$\mathbf{w}(n) = [w_o(n) \quad w_1(n) \quad \cdots \quad w_{L-1}(n)]^{\mathrm{T}}. \tag{16}$$

With these notations, the filter output is

$$y(n) = \mathbf{w}^{\mathrm{T}}(n)\mathbf{x}(n). \tag{17}$$

The sound pressure $p_e(n)$ and particle velocity $u_e(n)$ at the error sensor can be expressed as

$$p_e(n) = p_o(n) + \mathbf{h}_p^{\mathrm{T}}(n)\mathbf{y}(n), \qquad u_e(n) = u_o(n) + \mathbf{h}_u^{\mathrm{T}}(n)\mathbf{y}(n), \tag{18a, b}$$

where $\mathbf{h}_p(n)$ and $\mathbf{h}_u(n)$ represent the vectors containing the first $N$ samples of impulse responses of auxiliary plants relating the filter output $y(n)$ to the pressure $p_e(n)$ and velocity $u_e(n)$,

$$\mathbf{h}_p(n) = [h_{p,0}(n) \quad h_{p,1}(n) \quad \cdots \quad h_{p,N-1}(n)]^{\mathrm{T}},$$
$$\mathbf{h}_u(n) = [h_{u,0}(n) \quad h_{u,1}(n) \quad \cdots \quad h_{u,N-1}(n)]^{\mathrm{T}}, \tag{19a, b}$$

and $\mathbf{y}(n)$ is a vector of the latest $N$ output samples,

$$\mathbf{y}(n) = [\, y(n) \quad y(n-1) \quad \cdots \quad y(n-N+1)]^{\mathrm{T}}. \tag{20}$$

If one assumes that the coefficients of weight vector vary slowly, relative to the time scale of the response of the system to be controlled, the pressure and velocity at the error sensor become

$$p_e(n) = p_o(n) + \mathbf{h}_p^{\mathrm{T}}(n)\mathbf{X}(n)\mathbf{w}(n), \qquad u_e(n) = u_o(n) + \mathbf{h}_u^{\mathrm{T}}(n)\mathbf{X}(n)\mathbf{w}(n), \tag{21a, b}$$

where $\mathbf{X}(n)$ is a $N \times L$ matrix of the input signals,

$$\mathbf{X}(n) = [\mathbf{x}(n) \quad \mathbf{x}(n-1) \quad \cdots \quad \mathbf{x}(n-N+1)]^{\mathrm{T}}. \tag{22}$$

If one replaces the auxiliary plants $\mathbf{h}_p(n)$ and $\mathbf{h}_u(n)$ with the appropriate estimates $\hat{\mathbf{h}}_p(n)$ and $\hat{\mathbf{h}}_u(n)$, then equations (21a) and (21b) can be written as

$$p_e(n) = p_o(n) + \mathbf{w}^{\mathrm{T}}(n)\mathbf{r}_p(n), \qquad u_e(n) = u_o(n) + \mathbf{w}^{\mathrm{T}}(n)\mathbf{r}_u(n), \tag{23a, b}$$

where $\mathbf{r}_p(n)$ and $\mathbf{r}_u(n)$ are the filtered-$x$ signal vectors $\mathbf{r}_p(n)$ and $\mathbf{r}_u(n)$,

$$\mathbf{r}_p(n) = \mathbf{X}^{\mathrm{T}}(n)\hat{\mathbf{h}}_p(n), \qquad \mathbf{r}_u(n) = \mathbf{X}^{\mathrm{T}}(n)\hat{\mathbf{h}}_u(n), \tag{24a, b}$$

The mean active intensity at the error sensor ($I_a$), that is, the cost function to be minimized, is given by

$$J = I_a = \mathrm{E}[\, p_e(n)u_e(n)] = R_{peue}(\tau = 0), \tag{25}$$

where $R_{peue}(\tau)$ is the cross-correlation function between the pressure and velocity. It is noteworthy that the present cost function is the product of the two different physical quantities, pressure and velocity. Therefore, it is not possible simply to apply the (filtered-$x$) LMS adaptive algorithm [10], which is useful when a cost function is squared error or sum of squared errors. The active intensity expressed in the form of cross-correlation can be rewritten by the cross-spectral density function ($S_{peue}(\omega)$),

$$R_{peue}(\tau = 0) = \int_{-\infty}^{\infty} S_{peue}(\omega)\, \mathrm{d}\omega = \int_{0}^{\infty} 2\ \mathrm{Re}\,[S_{peue}(\omega)]\, \mathrm{d}\omega, \tag{26}$$

since the real part of the cross-spectral density function is even symmetric and the imaginary part is odd symmetric. From equations (9a), (11a) and (26), one can deduce that the mean active sound intensity at the downstream error sensor of duct is non-negative, $R_{peue}(0) \geqslant 0$, since all the frequency contents of the active intensity are non-negative, $2\ \mathrm{Re}\,[S_{peue}(\omega)] \geqslant 0$, under the physical termination condition $|R_t| \leqslant 1$.

To proceed with the derivation of the adaptive filtering algorithm, one can first examine the dependence of the cost function $J$ on the tap-weight vector $\mathbf{w}$. For convenience, consider $J = \{\mathrm{E}[\, p_e(n)u_e(n)] + \mathrm{E}[u_e(n)p_e(n)]\}/2$. Using equations (23a) and (23b), one has

$$\begin{aligned} J &= \tfrac{1}{2}\mathrm{E}[2p_o(n)u_o(n) + 2\mathbf{w}^{\mathrm{T}}\mathbf{r}_u(n)p_o(n) + 2\mathbf{w}^{\mathrm{T}}\mathbf{r}_p(n)u_o(n) + \mathbf{w}^{\mathrm{T}}\mathbf{r}_p(n)\mathbf{r}_u^{\mathrm{T}}(n)\mathbf{w} + \mathbf{w}^{\mathrm{T}}\mathbf{r}_u(n)\mathbf{r}_p^{\mathrm{T}}(n)\mathbf{w}] \\ &= \mathrm{E}[\, p_o(n)u_o(n)] + \mathbf{w}^{\mathrm{T}}\mathrm{E}[\mathbf{r}_u(n)p_o(n)] + \mathbf{w}^{\mathrm{T}}\mathrm{E}[\mathbf{r}_p(n)u_o(n)] \\ &\quad + \tfrac{1}{2}\mathbf{w}^{\mathrm{T}}\mathrm{E}[\mathbf{r}_p(n)\mathbf{r}_u^{\mathrm{T}}(n)]\mathbf{w} + \tfrac{1}{2}\mathbf{w}^{\mathrm{T}}\mathrm{E}[\mathbf{r}_u(n)\mathbf{r}_p^{\mathrm{T}}(n)]\mathbf{w} \\ &= C_{pouo} + \mathbf{w}^{\mathrm{T}}\mathbf{p}_{rupo} + \mathbf{w}^{\mathrm{T}}\mathbf{p}_{rpuo} + \tfrac{1}{2}\mathbf{w}^{\mathrm{T}}\mathbf{R}_{rpru}\mathbf{w} + \tfrac{1}{2}\mathbf{w}^{\mathrm{T}}\mathbf{R}_{rurp}\mathbf{w} \\ &= C_{pouo} + \mathbf{w}^{\mathrm{T}}\mathbf{p}_{rupo} + \mathbf{w}^{\mathrm{T}}\mathbf{p}_{rpuo} + \tfrac{1}{2}\mathbf{w}^{\mathrm{T}}(\mathbf{R}_{rpru} + \mathbf{R}_{rurp})\mathbf{w}, \end{aligned} \tag{27}$$

where $C_{pouo} = \mathrm{E}[\, p_o(n)u_o(n)]$ is the covariance between $p_o(n)$ and $u_o(n)$, $\mathbf{p}_{rupo} = \mathrm{E}[\mathbf{r}_u(n)p_o(n)]$ is the cross-correlation vector between the filtered-$x$ vector $\mathbf{r}_u(n)$ and $p_o(n)$, $\mathbf{p}_{rpuo} = \mathrm{E}[\mathbf{r}_p(n)u_o(n)]$ is the cross-correlation vector between the filtered-$x$ vector $\mathbf{r}_p(n)$ and $u_o(n)$, and $\mathbf{R}_{rpru} = \mathrm{E}[\mathbf{r}_p(n)\mathbf{r}_u^{\mathrm{T}}(n)]$ and $\mathbf{R}_{rurp} = \mathrm{E}[\mathbf{r}_u(n)\mathbf{r}_p^{\mathrm{T}}(n)]$ are the cross-correlation matrices between the filtered-$x$ vectors $\mathbf{r}_p(n)$ and $\mathbf{r}_u(n)$ respectively. The sum of the cross-correlation matrices $(\mathbf{R}_{rpru} + \mathbf{R}_{rurp})$ is non-negative, $\mathbf{w}^{\mathrm{T}}(\mathbf{R}_{rpru} + \mathbf{R}_{rurp})\mathbf{w} \geqslant 0$, since the cost function is always non-negative for any weight vector $\mathbf{w}$ as previously stated ($J \geqslant 0$). This equation, therefore, essentially shows that the present cost function (mean active intensity in the downstream part of the duct) is a positive quadratic function of the tap-weight vector which has a unique optimum.

The gradient of the cost function ($\nabla$) can be expressed as

$$\nabla = \partial \mathbf{J}/\partial \mathbf{w} = \mathbf{p}_{rupo} + \mathbf{p}_{rpuo} + (\mathbf{R}_{rpru} + \mathbf{R}_{rurp})\mathbf{w}. \tag{28}$$

The optimal weight vector to minimize the cost function can be obtained by setting $\nabla = 0$:

$$\mathbf{w}^* = -(\mathbf{R}_{rpru} + \mathbf{R}_{rurp})^{-1}(\mathbf{p}_{rupo} + \mathbf{p}_{rpuo}). \tag{29}$$

At time $n$, the cost function $J(n)$ with adjustable weight vector $\mathbf{w}(n)$ can be expressed as

$$J(n) = C_{pouo} + \mathbf{w}^{\mathrm{T}}(n)\mathbf{p}_{rupo} + \mathbf{w}^{\mathrm{T}}(n)\mathbf{p}_{rpuo} + \tfrac{1}{2}\mathbf{w}^{\mathrm{T}}(n)(\mathbf{R}_{rpru} + \mathbf{R}_{rurp})\mathbf{w}(n). \tag{30}$$

If one applies the method of steepest descent, the updated value of the tap-weight vector at time $n + 1$ can be computed as

$$\mathbf{w}(n + 1) = \mathbf{w}(n) - \mu\nabla(n), \tag{31}$$

where $\mu$ is a positive constant, and $\nabla(n)$ is the value of the gradient vector at time $n$. Differentiation of $J(n)$ in equation (30) by $\mathbf{w}(n)$ gives

$$\nabla(n) = \frac{\partial J(n)}{\partial \mathbf{w}(n)} = \mathbf{p}_{rupo} + \mathbf{p}_{rpuo} + (\mathbf{R}_{rpru} + \mathbf{R}_{rurp})\mathbf{w}(n). \tag{32}$$

If it were possible to measure the true gradient vector $\nabla(n)$ at each iteration, and if the step-size parameter $\mu$ is suitably chosen, then the tap-weight vector computed by the steepest descent algorithm would indeed converge to the optimal Wiener solution. In reality, however, exact measurements of the gradient vector are not possible, since this requires prior knowledge of both the cross-correlation matrices $\mathbf{R}_{rpru}$ and $\mathbf{R}_{rurp}$ and the cross-correlation vectors $\mathbf{p}_{rupo}$ and $\mathbf{p}_{rpuo}$. Consequently, the gradient vector must be *estimated* from the available data.

A realizable estimation method is to use a running time average instead of the ensemble average associated with the derivative. That is, one first defines an unbiased estimate of the cost function as a finite temporal average,

$$\hat{J}(n) = \frac{1}{M}\sum_{i=n}^{n+M-1} p_e(i)u_e(i), \tag{33}$$

where $M$ is an average step. The values assigned to this $M$-step record depend on the type of data windowing employed: for example, a rectangular window. During this interval $n \leqslant i \leqslant n + M + 1$, the tap-weight vector is held constant. Therefore, the gradient vector can be estimated by

$$\hat{\nabla}(n) = \frac{\partial}{\partial \mathbf{w}(n)}\left\{\frac{1}{M}\sum_{i=n}^{n+M-1} p_e(i)u_e(i)\right\} = \frac{1}{M}\sum_{i=n}^{n+M-1}\frac{\partial\{\,p_e(i)u_e(i)\}}{\partial \mathbf{w}(i)}$$

$$= \frac{1}{M}\sum_{i=n}^{n+M-1}\left\{p_e(i)\frac{\partial u_e(i)}{\partial \mathbf{w}(i)} + u_e(i)\frac{\partial p_e(i)}{\partial \mathbf{w}(i)}\right\}. \tag{34}$$

Substitution of equations (23a) and (23b) into equation (34) gives

$$\hat{\nabla}(n) = \frac{1}{M}\sum_{i=n}^{n+M-1}\{\,p_e(i)\mathbf{r}_u(i) + u_e(i)\mathbf{r}_p(i)\}. \tag{35}$$

Therefore, the tap-weight adaptation is given by

$$\mathbf{w}(n) = \mathbf{w}(n+1) = \cdots = \mathbf{w}(n+M-1), \tag{36a}$$

$$\mathbf{w}(n+M) = \mathbf{w}(n) - \mu\hat{\mathbf{V}}(n) = \mathbf{w}(n) - \frac{\mu}{M}\sum_{i=n}^{n+M-1}\{p_e(i)\mathbf{r}_u(i) + u_e(i)\mathbf{r}_p(i)\}$$

$$= \mathbf{w}(n) - \mu'\sum_{i=n}^{n+M-1}\{p_e(i)\mathbf{r}_u(i) + u_e(i)\mathbf{r}_p(i)\}, \tag{36b}$$

where $\mu'$ is a positive adaptation coefficient replacing the factor $\mu/M$.

This result is identical with the adaptive filtering algorithm for active absorbing power control of the control source [11]. However, the above adaptive filtering procedure still requires a lengthy averaging process at each iteration of which the averaging step ($M$) is essentially involved with the period of the lowest frequency noise component of interest and the sampling period. That is, the averaging step $M$ times the sampling period should be larger than, at least, the half period of the lowest frequency noise component of interest (since the sound intensity has second harmonic frequency components of the pressure or velocity signal) to achieve a reliable gradient estimation in the adaptive filtering.

An alternative approach is to use the gradient of the instantaneous $p_e(n)u_e(n)$ (the instantaneous sound intensity) to update each of the filter coefficients at every sample time, which is similar to the basic idea of the well-known LMS algorithm [10]. In this case, the gradient estimator can be obtained as

$$\hat{\mathbf{V}}(n) = \frac{\partial\{p_e(n)u_e(n)\}}{\partial\mathbf{w}(n)} = p_e(n)\frac{\partial u_e(n)}{\partial\mathbf{w}(n)} + u_e(n)\frac{\partial p_e(n)}{\partial\mathbf{w}(n)}$$

$$= p_e(n)\mathbf{r}_u(n) + u_e(n)\mathbf{r}_p(n). \tag{37}$$

Therefore the adaptive filtering law becomes

$$\mathbf{w}(n+1) = \mathbf{w}(n) - \mu\{p_e(n)\mathbf{r}_u(n) + u_e(n)\mathbf{r}_p(n)\}. \tag{38}$$

As a limiting case, if one deals with an infinite duct without reflecting waves, then $u_e(n) = p_e(n)/\rho c$ and $\mathbf{r}_u(n) = \mathbf{r}_p(n)/\rho c$. In this case, the adaptive algorithm described by equation (38) becomes the well-known filtered-$x$ LMS algorithm [10] which is widely used for local sound pressure control. However, in order to apply this method successfully to the present problem; active control of active sound intensity in the partially reactive field due to the open ended termination, it is essential to check *if the weight vector will converge to the true optimal solution for the active intensity control, at least in the mean, or not*. This convergence is checked and the adaptive algorithm is proved to be stable in the Appendix.

## 5. EXPERIMENT

To compare the active intensity control with the local sound pressure control, which can be influenced by sensor position and performance degradation due to the poor observability problem, as previously stated, real-time experiments were performed for the reduction of radiating noise.

### 5.1. EXPERIMENTAL SET-UP

A schematic diagram of the experimental system is shown in Figure 3. Experiments were conducted with a 5 mm thick acrylic plastic circular duct of diameter $D = 0{\cdot}13$ m and

length $L = 2{\cdot}77$ m. The cut-on frequency of the first higher order mode ($f_c$) is 1·545 kHz. A primary noise source at $x_p = 0$ m and a secondary source at $x_s = 1$ m were both 4 inch diameter loudspeakers, and the primary excitation was normally driven to produce a duct sound pressure level of 65–95 dB in the plane wave frequency range $f = 100$–$500$ Hz.

Sound pressure and particle velocity signals which are necessary for active intensity control were obtained by a sound intensity probe, Brüel and Kjaer (B&K) 3520 composed of two calibrated and phase-matched pressure microphones, B&K 4181, 1/2 in, with a spacing of 5 cm. The phase mismatch of the second microphone relative to the first microphone was positive and less than 0·02° in the frequency range of interest. The analog conversion from two pressure signals ($p_A(t)$ and $p_B(t)$) to pressure ($p_e(t)$) and velocity ($u_e(t)$) at the error sensor location was done by the well-known finite difference approximation method [14] based on the Euler equation with a B&K sound intensity analyzer type 4433.

The intensity error sensor was located on the duct central axis at $x_e = 2{\cdot}17$ m downstream of the secondary source. The reason why the error sensor was located on the central axis of the cross-section of the duct was to avoid the near field effect of the secondary source as soon as possible since the first higher order mode by the secondary source is a circumferential mode of which the nodal line crosses the central point of the duct cross-section. The error sensor location from the secondary source location along the $x$-axis was selected based on the three-dimensional analysis result of the finite open ended circular duct which has a circular source on the cylindrical wall [15], and the criteria suggested by a previous study [16] which showed that the near field contribution due to higher order modes can be neglected provided the distance between the secondary source and error microphone is more than about four times the width of the duct and the frequencies are below 0·9 times the cut-on frequency of the higher order mode. In this experiment, $x_e - x_s = 1{\cdot}17 \text{ m} > 4 \times D = 4 \times 13 \text{ cm} = 52 \text{ cm}$, $f_c = 0{\cdot}9 \times 1{\cdot}545 \text{ kHz} = 1{\cdot}35$ kHz.

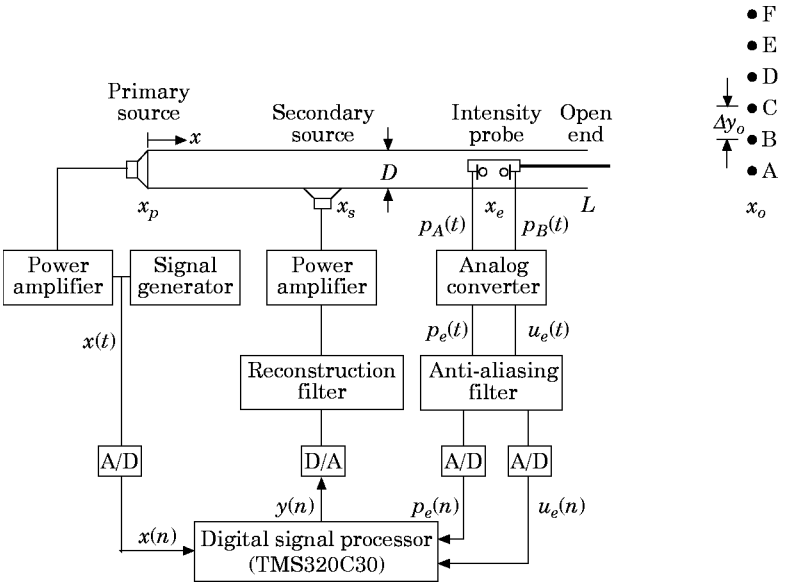


Figure 3. A schematic diagram of the experimental set-up. Duct length $L = 2{\cdot}77$ m, diameter $D = 0{\cdot}13$ m, primary source location $x_p = 0$ m, control source location $x_s = 1{\cdot}0$ m, error sensor location $x_e = 2{\cdot}17$ m, and for outer field monitoring positions ($A$–$F$) $x_o = (L + 1)$ m $= 3{\cdot}77$ m, $\Delta y_o = 0{\cdot}2$ m.

Radiated sound pressures from the duct exit were measured at six positions ($A$ to $F$) by a moving microphone (B&K 4165, 1/2 in) along the vertical line up to 45 degrees from the horizontal axis, 1 m from the duct exit.

### 5.2. CONSTRUCTION OF ADAPTIVE ATTENUATING FILTERS

An active control experiment of sound pressure in the test duct was conducted by the widely used time-domain filtered-$x$ LMS adaptive algorithm [10]. By using the generator signal as a reference input to the adaptive filter, the acoustic feedback problem, which is an unstable factor when the microphone signal upstream is used as a reference input, was eliminated in the experiment. The structure of the filtered-$x$ LMS algorithm is well-known, and therefore it will not be described in this paper.

For the active intensity control experiment for the test duct, the filtered-$x$ LMP algorithm described by equation (38) using the instantaneous intensity gradient estimate was applied. The impulse responses of the auxiliary plants $\mathbf{h}_p$ and $\mathbf{h}_u$ were identified off-line, prior to control optimization, with an LMS identification procedure.

Adaptive filtering algorithms to achieve sound pressure control and active intensity control were implemented on a TMS320C30 digital signal processor with sampling frequency 3 kHz.

### 5.3. DUCT CHARACTERISTICS

Before conducting the active control experiments, the sound pressure distribution and active sound intensity distribution in the test duct were measured, to obtain information about the acoustic characteristics of the duct.

In Figures 4(a) and 4(b) are illustrated the spectral and spatial distribution of sound pressure and active sound intensity before control, at 28 positions from $x = 0{\cdot}07$ m to $x = 2{\cdot}77$ m (duct end) with incremental spacing $\Delta x = 0{\cdot}1$ m. From Figure 4(a), one can see that the sound pressure distribution is strongly position-dependent. On the other hand, in Figure 4(b) it is shown that the active sound intensity distribution is less space-dependent than the sound pressure distribution. The measured active intensities for all frequencies in the duct were positive as expected, even if it is not explicitly shown in Figure 4(b) with the decibel scale. These two results correspond to the theoretical observations in section 3.

In Figure 5 are shown the sound pressure, active sound intensity distributions in the error sensor position $x_e = 2{\cdot}17$ m and the sound pressure distribution at the outer field position $A$ ($x_o = 3{\cdot}77$ m, $y_o = 0$ m). As previously stated, the error sensor location was selected with consideration of the near field effect. Nevertheless, one can see that the third resonance frequency component (276 Hz) is poorly observable by sound pressure measurement. On the other hand, all the frequency components emitted out of the duct exit are fully detected by the active sound intensity measurement. One can also see that the active sound intensity distribution is almost proportional to the exterior sound pressure distribution. This proportionality is essentially related to the termination condition of duct as previously stated in section 3.

### 5.4. RESULTS

Two typical frequency components were investigated in detail. The first frequency component is 276 Hz, which is the third resonance frequency in the frequency band 100–500 Hz. For this frequency component, the external sound field is poorly observable by measurement of duct pressure; on the other hand, it is well observable by measurement of active intensity, as shown in Figure 5. The second frequency component is the fourth resonance frequency, 337 Hz. For this one, both the measurements of sound pressure and

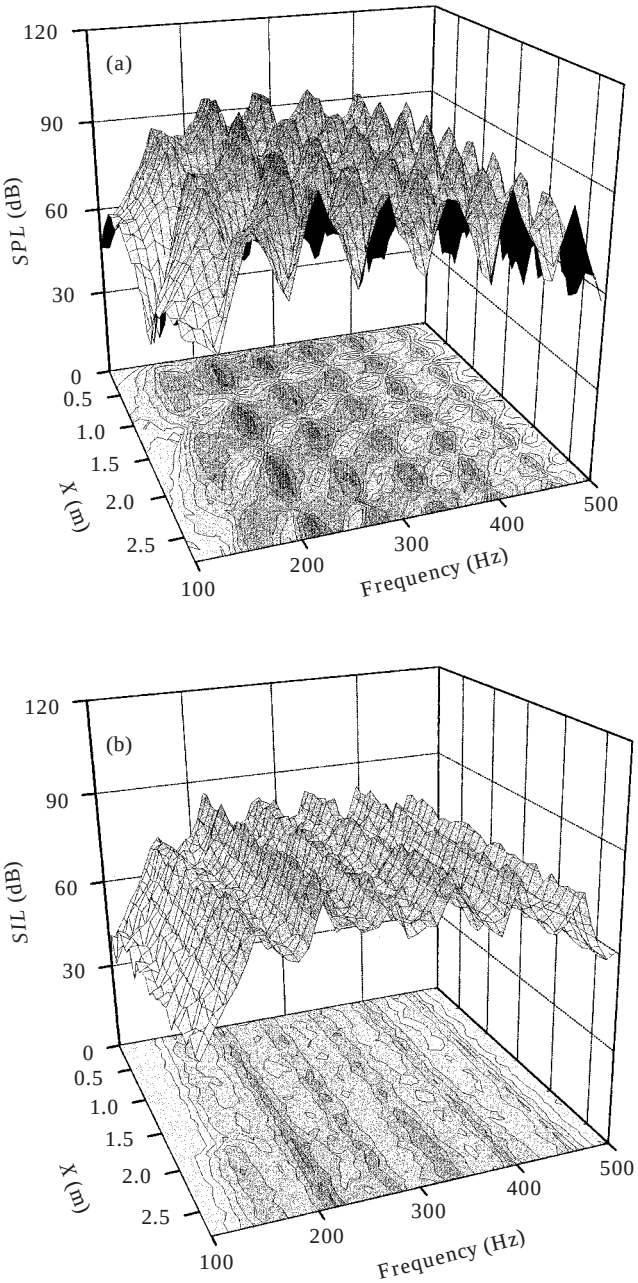


Figure 4. The spectral and spatial distribution of (a) the sound pressure and (b) the active sound intensity before control, at 28 positions from $x = 0{\cdot}17$ m to $x = 2{\cdot}77$ m (duct end) with a measurement interval $\Delta x = 0{\cdot}1$ m in the experimental test duct (see Figure 3).

active sound intensity have good observabilities. The adaptive filters for pressure control and active intensity control were allowed to converge fully, and then the adaptive filters were fixed while the measurements were made along the duct length.

In Figures 6(a) and 6(b) are shown the sound pressure level and sound intensity level in the duct for the first frequency component (276 Hz) respectively, before and after sound pressure control and active intensity control. For this frequency, one can see that the active

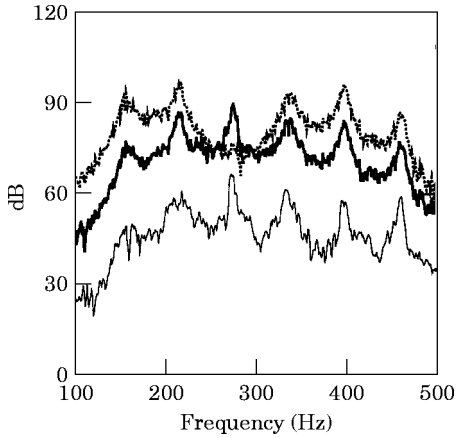


Figure 5. The spectral distribution of the sound pressure ( · · · · ) and the active sound intensity ( ) at the error sensor position ($x_e$) in the test duct (see Figure 3) before control, and the sound pressure distribution (—) emitted out of the duct end at the outer monitoring position $A$ ($x_o = 3{\cdot}77$ m, $y_o = 0$ m) before control.

control of sound pressure which has poor observability gives little reductions in both sound pressure level and sound intensity level downstream. On the other hand, the active intensity control which has good observability gives much better control results than the sound pressure control. In Figures 7(a) and 7(b) are shown the sound pressure level and sound intensity level in the duct respectively, for the second frequency component (337 Hz). For this frequency component, which is well observable by both measurement of sound pressure and sound intensity, one can see that the two control methods give similar large reduction results, as expected.

Since the ultimate purpose of the active control in this work is exterior field control, sound pressure levels were measured at six positions ($A$–$F$ in Figure 3) in the exterior field of the open ended test duct, to assess the control performances. The results are shown in Table 1. For the first frequency component (276 Hz), the attenuation of the sum of the sound pressure levels at the outer six positions is far larger with sound intensity control

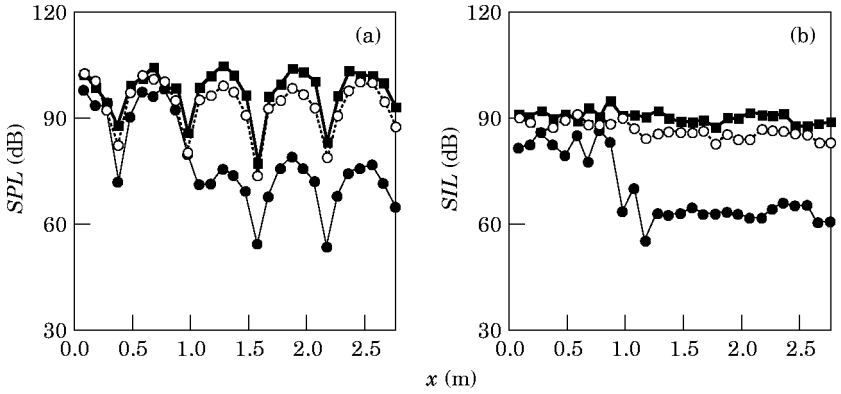


Figure 6. Spatial change of (a) the sound pressure level and (b) the active sound intensity level in the experimental test duct (see Figure 3) for the third resonance frequency (276 Hz) in the frequency band 100–500 Hz, before and after the sound pressure control and active intensity control. —■—, Before control; —○—, pressure control; —●—, active intensity control.

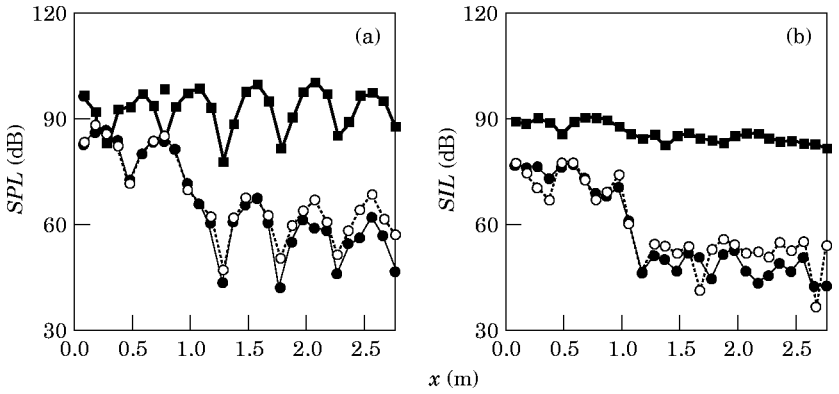


Figure 7. Spatial change of (a) the sound pressure level and (b) the active sound intensity level in the experimental test duct (see Figure 3) for the fourth resonance frequency (337 Hz) in the frequency band 100–500 Hz, before and after the sound pressure control and active intensity control. Key as Figure 6.

than with sound pressure control. One can also see that the attenuation levels with pressure control and intensity control are similar for the second frequency component (337 Hz). However, the sound intensity control gives a little more attenuation level than the sound pressure control in this case too.

## 6. CONCLUDING REMARKS

In this paper, an active intensity control strategy has been proposed to control the radiated noise out of a duct, based on a theoretical analysis as well as experimental investigation.

One of the features of the active intensity control strategy is that the control performance is maintained regardless of the sensor location, unlike with the conventional local pressure control method, at an interior downstream or exterior field position. This is because the active intensity distribution at the downstream is not space-dependent if it is plane wave. On the other hand, the sound pressure distributions at interior and exterior field points are acoustically space-dependent: that is, one has standing wave patterns and directivity patterns. It also turned out that the theoretical optimal filter for the active intensity control takes on a form of causal transversal filter, which does not demand knowledge of the non-causal part nor does it not depend on the downstream termination condition. That is, provided that the number of digital filter coefficients is large enough to model the main acoustic plant, one can expect nearly complete cancellation of the radiated duct noise.

TABLE 1

*Sum of the sound pressure levels at six positions (A–F) in the exterior field of open ended test duct (Figure 3) before and after pressure control and active intensity control*

| Investigated frequency (Hz) | Sum of *SPL* values before control (dB) | Sum of *SPL* values after pressure control (attenuation) (dB) | Sum of *SPL* values after intensity control (attenuation) (dB) |
|---|---|---|---|
| 276 | 70·5 | 67·1 (3·4) | 48·8 (21·7) |
| 337 | 65·3 | 43·1 (22·2) | 40·4 (24·9) |

From a practical signal processing viewpoint, it was suggested and proved that the digital filtering for the active intensity control can be achieved by the time-domain filtered-$x$ LMP (least-mean-product) adaptive algorithm with instantaneous sound intensity, which is far simpler than the time-domain algorithm using finite temporal averaged intensity or frequency-domain algorithm using the active parts of the sound intensity in finite Fourier transformed domain.

Experiments with an open ended duct were performed to compare the active intensity control performance with that of sound pressure control. The former control implementation used the suggested filtered-$x$ LMP algorithm and the latter the filtered-$x$ LMS algorithm. From the experimental results, it was shown that the exterior sound field was much more observable when sensing the active intensity in the duct than just sound pressure. It was also concluded that the active intensity control performances are superior to the sound pressure control ones.

In practical implementation, the present active intensity control system implicity requires a sound intensity detector. If a two-microphone method is used, closely spaced two microphones such as the commercially available intensity probe can be used. In general, the two microphone technique for the measurement of sound intensity is subject to errors which arise from finite difference approximations which are inherent in the transduction principle employed, and from imperfections of the measurement systems. These errors are also functions of the type of acoustic field under investigation. Therefore, the measurement accuracy of active sound intensity in the open end duct system which has a partially reactive sound field, would be position-dependent. However, some errors in the estimate of active sound intensity level, that is, overestimation or underestimation of active sound intensity level, can be tolerated, since one is interested in *controlling* the magnitude of active sound intensity rather than in *mapping* the sound field. The most important error from the viewpoint of active control is the sign reversal problem which can occur due to channel phase mismatch of the measurement system. That is, if the sign of the estimated active sound intensity (due to the control source alone) is negative in the duct downstream due to the phase mismatch error, the present active control strategy would fail, since the shape of the error performance function in equation (30) becomes negative quadratic: $\mathbf{w}^{\mathrm{T}}(\mathbf{R}_{rpru} + \mathbf{R}_{rurp})\mathbf{w} < 0$. In a standing wave field with standing wave ratio $R$, the sign reversal can occur when the phase mismatch of the second microphone relative to the first one is negative and the magnitude of the phase mismatch is larger than $k\Delta r/R$ where $\Delta r$ is the separation distance [17]. (On the other hand, if the phase mismatch has a positive value, then the sign reversal does not happen even if the intensity level is overestimated or underestimated.) For example, if the standing wave ratio is 13 dB, the magnitude of the reflection coefficient is 0·9, the minimum frequency of interest is 200 Hz, and the separation distance is 5 cm, then the magnitude of the negative phase mismatch should be at least less than $0{\cdot}5^{\circ}$, to ensure a correct sign. Therefore it is necessary to use well phase-matched microphones, and to check the sign of the active intensity before control in the frequency band of interest.

## ACKNOWLEDGMENTS

The authors would like to thank Yong-Joe Kim of KAIST, for his assistance in the experiment. Part of this work was presented at the 127th meeting of the Acoustical Society of America, MIT, Cambridge, Massachusetts (June 1994) (*Journal of the Acoustical Society of America* **95**, Pt. 2, 2932 (1994)). We also thank the editor, P. E. Doak, and two anonymous reviewers for their criticisms and suggestions on the previous version of this paper.

## REFERENCES


1. M. J. M. Jessel and G. A. Mangiante 1972 *Journal of Sound and Vibration* **27**, 383–390. Active sound absorber in an air conditioning duct.
2. J. Tichy, G. E. Warnaka and L. A. Poole 1984 *Transactions of the American Society of Mechanical Engineers Journal of Vibration, Acoustics, Stress, and Reliability in Design* **106**, 399–404. A study of active control of noise in ducts.
3. R. F. La Fontaine and I. C. Shepherd 1985 *Journal of Sound and Vibration* **100**, 569–579. The influence of waveguide reflections and system configuration on the performance of an active noise attenuator.
4. A. R. D. Curtis, P. A. Nelson, S. J. Elliott and A. J. Bullmore 1987 *Journal of the Acoustical Society of America* **81**, 624–631. Active suppression of acoustic resonance.
5. A. R. D. Curtis, P. A. Nelson and S. J. Elliott 1990 *Journal of the Acoustical Society of America* **88**, 2265–2268. Active reduction of a one-dimensional enclosed sound field: an experimental investigation of three control strategies.
6. S. J. Elliott, P. Joseph, P. A. Nelson and M. E. Johnson 1991 *Journal of the Acoustical Society of America* **90**, 2501–2511. Power output minimization and power absorption in active control of sound.
7. A. C. Zander and C. H. Hansen 1993 *Journal of the Acoustical Society of America* **94**, 841–848. A comparison of error sensor strategies for the active control of duct noise.
8. S. J. Stell and R. J. Bernard 1994 *Journal of Sound and Vibration* **173**, 179–196. Active control of sound in acoustic waveguides, part I: theory.
9. S. J. Stell and R. J. Bernard 1994 *Journal of Sound and Vibration* **173**, 197–215. Active control of sound in acoustic waveguides, part II: considerations for implementation in ducts.
10. B. Widrow and S. D. Stearns 1985 *Adaptive Signal Processing*. Englewood Cliffs, NJ: Prentice-Hall.
11. J. Hald 1991 *Proceedings of the International Symposium on Active Control of Sound and Vibration, Tokyo* 285–290. A power controlled active noise cancellation technique.
12. D. C. Swanson 1994 *Proceedings of Inter-Noise* 94, *Yokohama*, 1253–1258. Active control of acoustic intensity using a frequency domain filtered-$x$ algorithm.
13. S. D. Sommerfeldt and P. J. Nashif 1994 *Journal of the Acoustical Society of America* **96**, 300–306. An adaptive filtered-$x$ algorithm for energy-based active control.
14. F. J. Fahy 1989 *Sound Intensity*. London: Elsevier Applied Science.
15. S.-W. Kang and Y.-H. Kim 1995 *Journal of Sound and Vibration* **181**, 765–780. Green function analysis of the acoustic field in a finite three-port circular chamber.
16. J. Kazakia 1986 *Journal of Sound and Vibration* **110**, 495–509. A study of active attenuation of broadband noise.
17. R. W. Guy and J. Li 1992 *Journal of the Acoustical Society of America* **92**, 2709–2715. Intensity measurements in the presence of standing waves.


## APPENDIX: CONVERGENCE OF FILTERED-$x$ LEAST-MEAN-PRODUCT ALGORITHM

Taking the expected value of both sides of equation (38) yields the difference equation

$$\mathrm{E}[\mathbf{w}(n+1)] = \mathrm{E}[\mathbf{w}(n)] - \mu \mathrm{E}[\, p_e(n)\mathbf{r}_u(n) + u_e(n)\mathbf{r}_p(n)]. \tag{A1}$$

Substituting equations (23a) and (23b) into equation (A1) gives

$$\begin{aligned}\mathrm{E}[\mathbf{w}(n+1)] &= \mathrm{E}[\mathbf{w}(n)] - \mu \mathrm{E}[\{p_o(n) + \mathbf{w}^{\mathrm{T}}(n)\mathbf{r}_p(n)\}\mathbf{r}_u(n) + \{u_o(n) + \mathbf{w}^{\mathrm{T}}(n)\mathbf{r}_u(n)\}\mathbf{r}_p(n)] \\ &= \mathrm{E}[\mathbf{w}(n)] - \mu\{\mathrm{E}[p_o(n)\mathbf{r}_u(n)] + \mathrm{E}[\mathbf{w}^{\mathrm{T}}(n)\mathbf{r}_p(n)\mathbf{r}_u(n)] + \mathrm{E}[u_o(n)\mathbf{r}_p(n)] \\ &\quad + \mathrm{E}[\mathbf{w}^{\mathrm{T}}(n)\mathbf{r}_u(n)\mathbf{r}_p(n)]\}. \end{aligned} \tag{A2}$$

From equation (38), one can see that the weight vector $\mathbf{w}(n)$ is a function only of the past filtered input vectors $\mathbf{r}_p(n-1), \mathbf{r}_p(n-2), \ldots, \mathbf{r}_p(0)$ and $\mathbf{r}_u(n-1), \mathbf{r}_u(n-2), \ldots, \mathbf{r}_u(0)$. If one assumes that successive input vectors $\mathbf{x}(n-1), \mathbf{x}(n-2), \ldots, \mathbf{x}(0)$ are independent as time goes on, then $\mathbf{w}(n)$ is independent of $\mathbf{r}_p(n)$ and $\mathbf{r}_u(n)$ since the successive filtered input

vectors are also independent respectively. Also, from equation (29) one has the optimum weight vector given as $\mathbf{w}^* = -(\mathbf{R}_{rpru} + \mathbf{R}_{rurp})^{-1}(\mathbf{p}_{rupo} + \mathbf{p}_{rpuo})$. Thus, equation (A2) becomes

$$\begin{aligned}\mathrm{E}[\mathbf{w}(n+1)] &= \mathrm{E}[\mathbf{w}(n)] - \mu\{\mathrm{E}[\mathbf{r}_u(n)p_o(n)] + \mathrm{E}[\mathbf{r}_u(n)\mathbf{r}_p^{\mathrm{T}}(n)]\mathrm{E}[\mathbf{w}(n)] + \mathrm{E}[\mathbf{r}_p(n)u_o(n)] \\ &\quad + \mathrm{E}[\mathbf{r}_p(n)\mathbf{r}_u^{\mathrm{T}}(n)]\mathrm{E}[\mathbf{w}(n)]\} \\ &= \mathrm{E}[\mathbf{w}(n)] - \mu\{\mathbf{p}_{rupo} + \mathbf{R}_{rurp}\mathrm{E}[\mathbf{w}(n)] + \mathbf{p}_{rpuo} + \mathbf{R}_{rpru}\mathrm{E}[\mathbf{w}(n)]\} \\ &= \mathrm{E}[\mathbf{w}(n)] - \mu\{\mathbf{p}_{rupo} + \mathbf{p}_{rpuo} + (\mathbf{R}_{rpru} + \mathbf{R}_{rurp})\mathrm{E}[\mathbf{w}(n)]\} \\ &= \mathrm{E}[\mathbf{w}(n)] - \mu\{-(\mathbf{R}_{rpru} + \mathbf{R}_{rurp})\mathbf{w}^* + (\mathbf{R}_{rpru} + \mathbf{R}_{rurp})\mathrm{E}[\mathbf{w}(n)]\}. \end{aligned} \tag{A3}$$

Upon subtracting the optimum weight $\mathbf{w}^*$ from both sides of equation (A3), and using the weight-error vector $\boldsymbol{\varepsilon}(n) = \mathbf{w}(n) - \mathbf{w}^*$, equation (A3) becomes

$$\mathrm{E}[\boldsymbol{\varepsilon}(n+1)] = \{\mathbf{I} - \mu(\mathbf{R}_{rpru} + \mathbf{R}_{rurp})\}\mathrm{E}[\boldsymbol{\varepsilon}(n)], \tag{A4}$$

where the matrix $(\mathbf{R}_{rpru} + \mathbf{R}_{rurp})$ is symmetric, since

$$\begin{aligned}(\mathbf{R}_{rpru} + \mathbf{R}_{rurp})^{\mathrm{T}} &= \mathrm{E}[\{\mathbf{r}_p(n)\mathbf{r}_u^{\mathrm{T}}(n) + \mathbf{r}_u(n)\mathbf{r}_p^{\mathrm{T}}(n)\}^{\mathrm{T}}] \\ &= \mathrm{E}[\{\mathbf{r}_u(n)\mathbf{r}_p^{\mathrm{T}}(n) + \mathbf{r}_p(n)\mathbf{r}_u^{\mathrm{T}}(n)\}] = \mathbf{R}_{rurp} + \mathbf{R}_{rpru}. \end{aligned} \tag{A5}$$

By using the unitary similarity transformation for a symmetric matrix, the cross-correlation matrix $(\mathbf{R}_{rpru} + \mathbf{R}_{rurp})$ can be diagonalized as

$$\mathbf{R}_{rpru} + \mathbf{R}_{rurp} = \mathbf{Q}\boldsymbol{\Lambda}\mathbf{Q}^{\mathrm{T}}. \tag{A6}$$

The unitary matrix $\mathbf{Q}$ has as its columns an orthogonal set of eigenvectors associated with the eigenvalues of the matrix $(\mathbf{R}_{rpru} + \mathbf{R}_{rurp})$. The matrix $\boldsymbol{\Lambda}$ is a diagonal matrix and has as its diagonal elements the eigenvalues $\lambda_1, \lambda_2, \ldots, \lambda_L$. These eigenvalues are all non-negative and real, since the matrix $(\mathbf{R}_{rpru} + \mathbf{R}_{rurp})$ is non-negative and symmetric.

Substituting equation (A6) in equation (A4), pre-multiplying both sides by $\mathbf{Q}^{\mathrm{T}}$ and using the property of the unitary matrix, $\mathbf{Q}^{\mathrm{T}} = \mathbf{Q}^{-1}$, one obtains

$$\mathrm{E}[\mathbf{Q}^{\mathrm{T}}\boldsymbol{\varepsilon}(n+1)] = \{\mathbf{I} - \mu\boldsymbol{\Lambda}\}\mathrm{E}[\mathbf{Q}^{\mathrm{T}}\boldsymbol{\varepsilon}(n)]. \tag{A7}$$

Upon defining an uncoupled principal co-ordinate vector as $\mathbf{v}(n) = \mathbf{Q}^{\mathrm{T}}\boldsymbol{\varepsilon}(n)$, the solution of equation (A7) becomes

$$\mathrm{E}[\mathbf{v}(n)] = \{\mathbf{I} - \mu\boldsymbol{\Lambda}\}^n\mathbf{v}(0), \tag{A8}$$

where $\mathbf{v}(0)$ is the initial weight vector in the principal-axis system. Therefore, one can deduce that the mean of $\mathbf{v}(n)$ converges to zero as $n$ approaches infinity, provided that the condition

$$0 < \mu < 2/\lambda_{max} \tag{A9}$$

is satisfied, where $\lambda_{max}$ is the largest eigenvalue of the cross-correlation matrix $(\mathbf{R}_{rpru} + \mathbf{R}_{rurp})$.

One can observe that this result is very similar to the convergence condition of the LMS algorithm [10]. In particular, the cross-correlation matrix $(\mathbf{R}_{rpru} + \mathbf{R}_{rurp})$ between the filtered-input particle velocity signal and the sound pressure signal has a role identical to that of the auto-correlation matrix of the input signal of the LMS algorithm. In other words, provided that the step-size parameter $\mu$ is set within the bounds defined by equation (A9), the mean of the tap-weight vector $\mathbf{w}(n)$ computed by using the filtered-$x$ LMP (least-mean-product) algorithm described by equation (38) converges to the optimum Wiener solution $\mathbf{w}^*$ as the number of iterations approaches infinity.